Astron. Nachr. / AN **328**, No. 1, 80 – 91 (2007) / **DOI** 10.1002/asna.200610707

Statistical properties of polarized radio continuum emission and effects of data processing

I. Mizeva[1], **W. Reich**[2,⋆], **P. Frick**[1], **R. Beck**[2], and **D. Sokoloff**[3]

[1] Institute of Continuous Media Mechanics, Korolyov str. 1, 614061 Perm, Russia
[2] Max-Planck-Institut für Radioastronomie, Auf dem Hügel 69, 53121 Bonn, Germany
[3] Department of Physics, Moscow State University, 119992 Moscow, Russia

Received 2006 Sep 18, accepted 2006 Nov 13
Published online 2006 Dec 31

Key words techniques: polarimetric – ISM: magnetic fields – radio continuum: galaxies – radio continuum: ISM

Polarized intensity and polarization angles are calculated from Stokes parameters Q and U in a nonlinear way. The statistical properties of polarized emission hold information about the structure of magnetic fields in a large range of scales, but the contributions of different stages of data processing to the statistical properties should first be understood. We use 1.4 GHz polarization data from the Effelsberg 100-m telescope of emission in the Galactic plane, near the plane and far out of the plane. We analyze the probability distribution function and the wavelet spectrum of the original maps in Stokes parameters Q, U and corresponding PI. Then we apply absolute calibration (i.e. adding the large-scale emission to the maps in Q and U), subtraction of polarized sources and subtraction of the positive bias in PI due to noise ("denoising"). We show how each procedure affects the statistical properties of the data. We find a complex behavior of the statistical properties for the different regions analyzed which depends largely on the intensity level of polarized emission. Absolute calibration changes the morphology of the polarized structures. The statistical properties change in a complex way: Compact sources in the field flatten the wavelet spectrum over a substantial range. Adding large-scale emission does not change the spectral slopes in Q and U at small scales, but changes the PI spectrum in a complex way. "Denoising" significantly changes the p.d.f. of PI and raises the entire spectrum. The final spectra are flat in the Galactic plane due to magnetic structures in the ISM, but steeper at high Galactic latitude and in the anticenter. For a reliable study of the statistical properties of magnetic fields and turbulence in the ISM based on radio polarization observations, absolute calibration and source subtraction are required.

1 Introduction

Observations of polarized synchrotron emission are the basis of our knowledge concerning magnetic fields in the Milky Way and in external galaxies. The large-scale component of magnetic fields in galaxies seems to be more or less understood (see Beck et al. 1996 and Beck 2006 for reviews), while the properties of small-scale magnetic fields and methods of their extraction from observational data still are much less clear. In external galaxies depolarization effects give indirect evidence for small-scale fields, but the resolution of present-day radio telescopes is insufficient to resolve them.

Observations of polarized emission from the Milky Way (see Reich 2006 for a review) hold the clue to understand small-scale fields. A wealth of polarization structures has been recently discovered (Gray 1998; Uyaníker et al. 1998; Uyaníker et al. 1999; Gaensler et al. 2001; Haverkorn et al. 2003a, 2003b) most of which are unrelated to features in the corresponding map of total intensity. However, it is sometimes difficult to decide which polarized small-scale structures in the maps reflect properties of the interstellar magnetic field or/and interstellar turbulence and which ones originate from observation noise, source subtraction, missing large-scale structures or background sources.

The observation method itself may also cause severe problems. Missing large-scale structure is a well-known problem for all interferometers, but also to some extent for single-dish telescopes, introduced by baseline setting at the edges of each map. This means that the size of a single-dish map determines the approximate scale of the largest structures included. The missing structures can be added with help of observations with smaller single-dish telescopes which allow to map larger regions or even the visible sky (Wolleben et al. 2006). While small-scale structures in the maps of Stokes parameters I, Q or U remain unchanged relative to their surroundings when adding large-scale structures, this does not hold for polarized intensity and polarization angle which are nonlinear functions of Q and U. For instance, the possibly most striking features in many published polarization maps, the depolarized "canals", could be due to turbulent structures in the ISM or may be caused by differential Faraday rotation (Shukurov & Berkhuijsen 2003; Haverkorn & Heitsch 2004; Fletcher & Shukurov 2006). On the other hand, it should be noted that such features are easily created in maps with missing low spatial

⋆ Corresponding author: wreich@mpifr-bonn.mpg.de

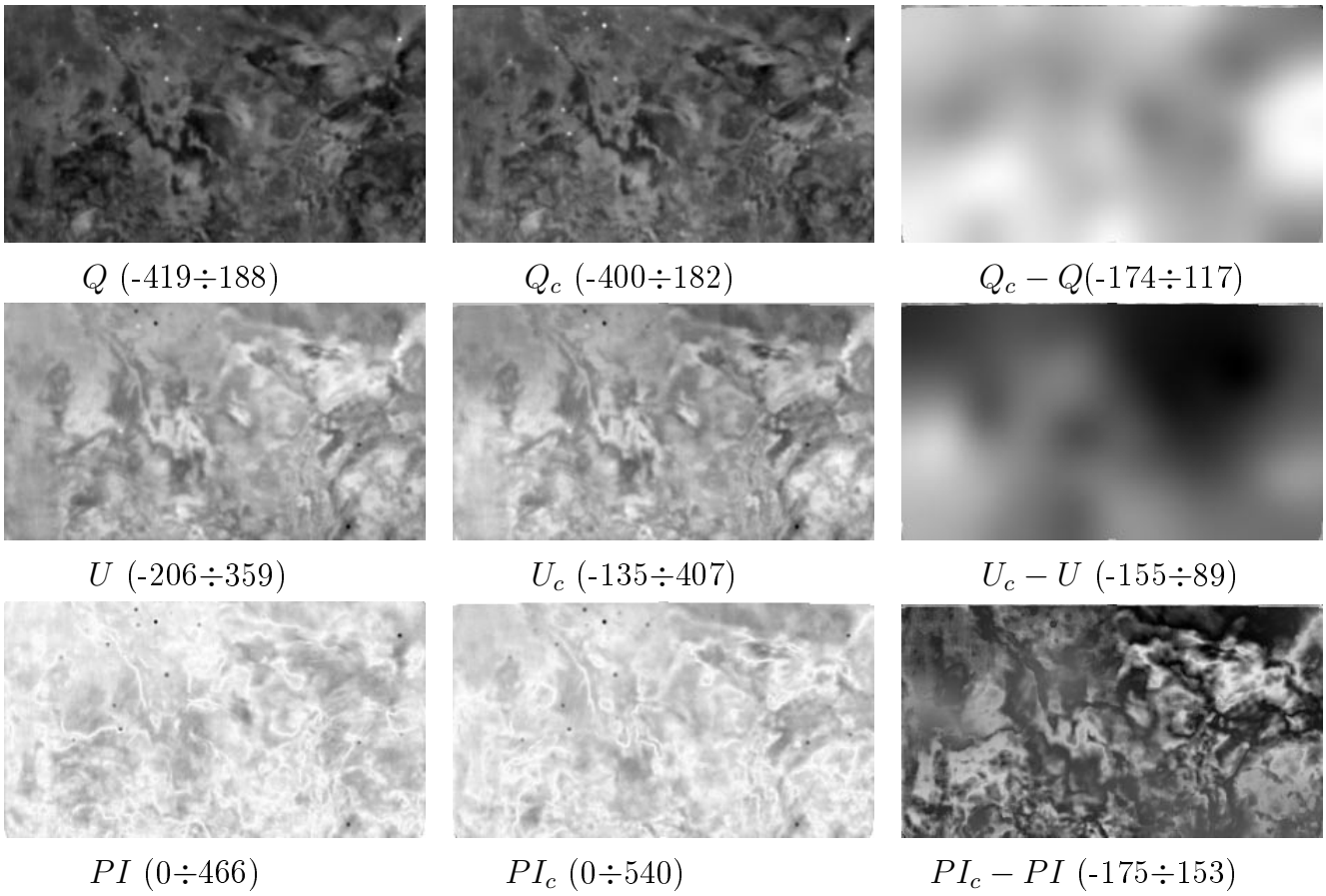

Fig. 1 Original (left column) and absolutely calibrated (center column, see Sect. 4.1) maps of Q, U and PI for the anticenter region (AC). The right column shows the difference of corresponding original and calibrated maps. The gray scale runs linearly from white (minimum intensity) to black (maximum intensity). For each map the minimum and maximum values are quoted.

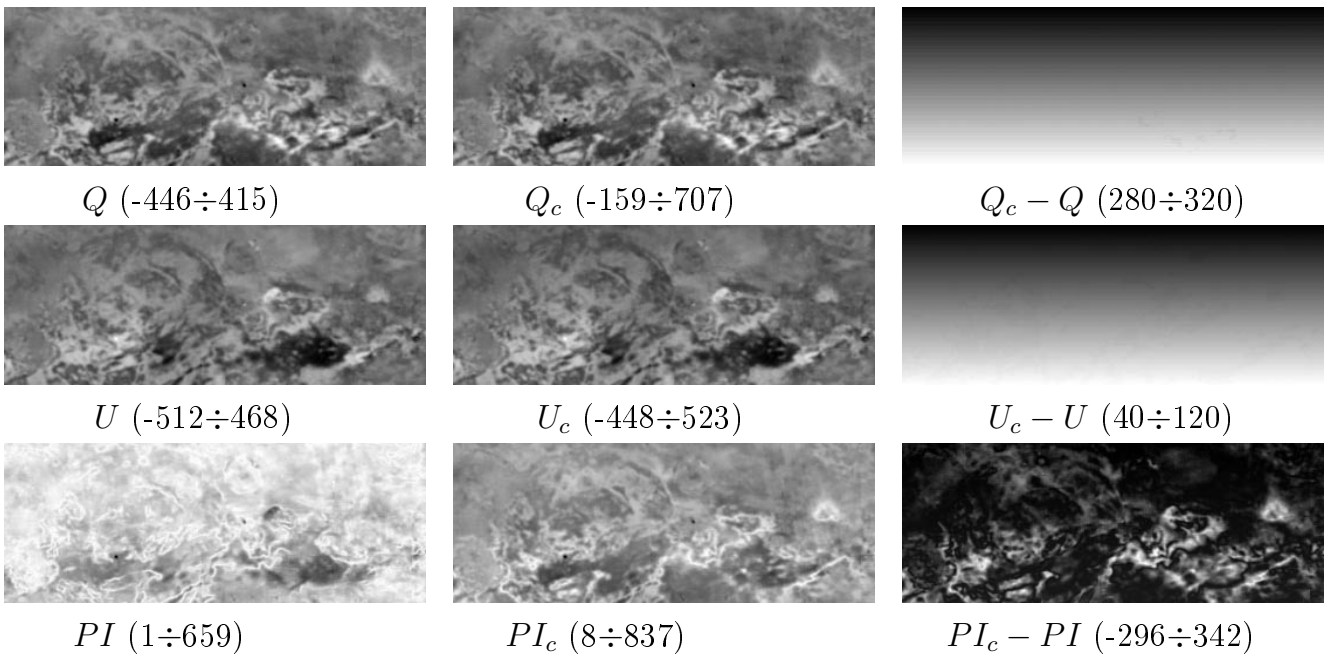

Fig. 2 Same as in Fig. 1, but for the Galactic plane region (GP).

frequencies and thus many "canals" disappear when large-scale emission is included (Reich 2006).

The properties of small-scale structures may be further affected by various sources of noise, either of instrumental origin or from the sky, for example from discrete radio sources. Discrete radio sources change the statistical properties of the Galactic diffuse emission. Low-level noise in the observed maps of Q and U leads to a positive bias in the map of polarized intensity PI, which is obtained by the nonlinear combination of Q and U.

In this paper we analyze a representative example of three regions from surveys of Galactic radio continuum emission obtained at 1.4 GHz with the Effelsberg 100-m telescope, two regions from the "Effelsberg Medium Latitude Survey" and one high-latitude region. For all three regions additional information on the missing large-scale emission is directly available or can be modeled. A brief description of the data is given in Sect. 2. We continue with a description of statistical properties of the maps which are useful for the understanding of the small-scale magnetic fields (Sect. 3). We discuss the effects of various steps of data processing, such as absolute calibration (Sect. 4.1), source subtraction (Sect. 4.2) and "denoising" (Sect. 4.3) on statistical properties of the radio polarization maps. We summarize our results in Sect. 5.

2 Properties of the selected regions

All observations of the selected regions were performed with the 100-m telescope of the MPIFR (Max-Planck-Institut für Radioastronomie) at Effelsberg at 1.4 GHz. The basic map parameters are listed in Table1. Two regions were taken from the "Effelsberg Medium Latitude Survey" (EMLS, as described by Uyaníker et al. 1998). The anticenter region (AC) from the survey was published by Uyaníker et al. (1999) and the Galactic plane section (GP) by Reich et al. (2004). The high latitude (HL) region was observed in the same way as the EMLS data (Reich et al. 2002). The data are scaled in mK or radio brightness temperature, T_b, based on well known calibration sources (Uyaníker et al. 1998).

We exploit three representative regions of the polarized Milky Way. AC is a cold region towards the Galactic anti-centre slightly off the Galactic plane. The dominating smooth diffuse emission in total intensity decreases with Galactic latitude and numerous extragalactic sources are visible (Uyaníker et al. 1999). The level of background emission above the cosmic microwave background varies from about 1 K to 1.3 K (Uyaníker et al. 1999, Fig. 14). For all maps the large-scale total intensity component is obtained by using data from the absolutely calibrated Stockert northern sky survey at 1.4 GHz (Reich 1982; Reich & Reich 1986). The Galactic plane region (GP) centered at $l = 162^\circ$ shows a number of well known supernova remnants and HII regions superimposed on diffuse emission with little structure (Reich et al. 2004). The level of Galactic total intensity emission in this region is about 1.3 K (Reich et al. 1997). The high latitude HL region (Reich et al. 2002) is almost structureless in total intensity and compact extragalactic sources are dominating. The level of Galactic emission in total intensity is about 0.5 K in this case (Reich 1982).

Table 1 Data characteristics: The first column indicates the region name and the center in Galactic coordinates, the second column gives the map size in pixels, the third one the size in Galactic longitude and latitude direction and the fourth column the reference. The pixel size of all maps is $4'$ and the beam size is $9.4'$.

Map center l, b (deg)	Map area (pix)	Map area (arcmin)	Reference
AC(200,9.4)	301×169	1200 × 672	Uyaníker et al. 1999
GP(162,0)	361×136	1440 × 540	Reich et al. 2004
HL(109,73)	76×76	300 × 300	Reich et al. 2002

The original maps in Stokes parameters Q and U and in polarized intensity $PI = \sqrt{Q^2 + U^2}$ are shown in Figs. 1–3 (left columns).

The missing large-scale structures in Q and U were recovered using different data sets. For the AC and the HL region we used the first coverage of the DRAO 1.4 GHz northern sky survey (Wolleben 2005). For the GP region we used Dwingeloo data (Brouw & Spoelstra 1976), which are largely undersampled. The data for the GP region required some modeling, since in the lower half of the map only very few Dwingeloo measurements were available indicating a smooth gradient in U and Q with Galactic latitude across the region (see Fig. 2). We note that meanwhile a new northern sky survey at 1.4 GHz has been completed (Wolleben et al. 2006). This survey uses the Dwingeloo data to find the absolute scale. A combination of the Effelsberg maps with this new survey was not attempted as only slightly different results are expected and the main objective of this study is to investigate the principle effects of absolute calibration on the structure distributions.

3 Small-scale structures characteristics: p.d.f. and spectra

We are interested in small-scale features in the magnetic field and the interstellar medium. Because the features of interest are thought to be random we have to extract some statistical quantities from the maps observed.

3.1 Probability distribution function

A straightforward tool for the statistical description of a map is a probability distribution function (p.d.f.) for a given variable, say, Q, i.e. $p(Q)$. We remind that $p(Q)\Delta Q$ is the relative number of pixels for which this Stokes parameter is in the range between Q and $Q + \Delta Q$. Of course, a p.d.f. can be introduced for other variables of interest, e.g. U and PI.

We present the p.d.f. for Q, U and PI for all three regions in Fig. 4. Note that the linear-log coordinates are

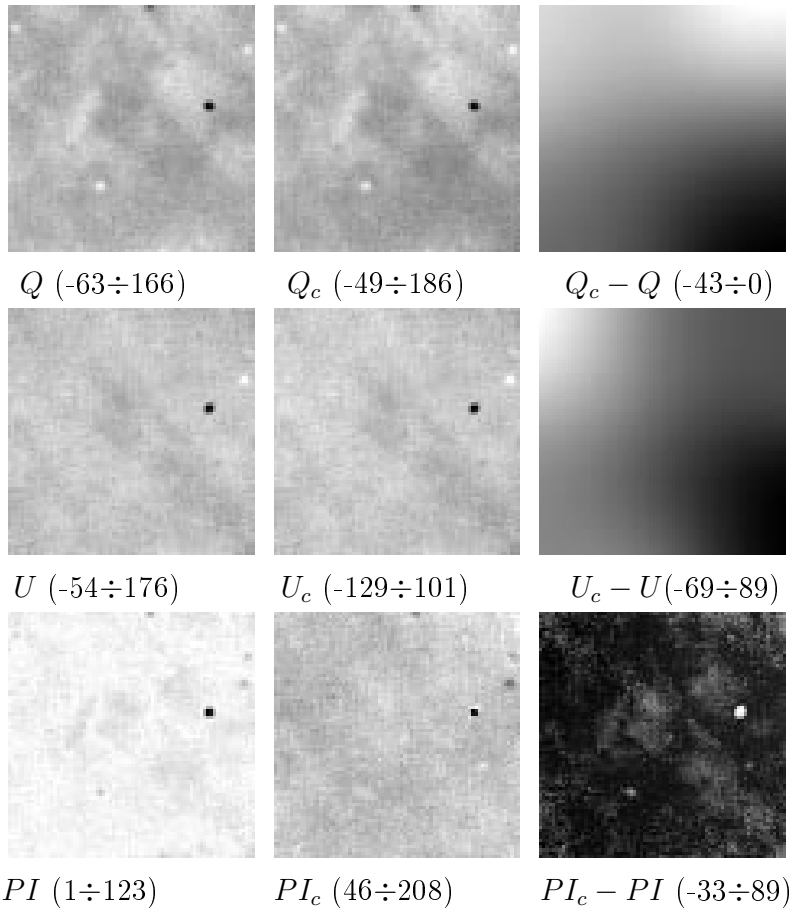

Fig. 3 Same as in Fig. 1, but for the high latitude region (HL).

used – in this presentation a Gaussian distribution gives a parabola. The Q and U distribution for the high latitude region HL have an approximately Gaussian p.d.f. For the "anticenter" region AC they are also quite close to the Gaussian shape but with larger widths. This means that the intensity of structures in polarized emission is substantially larger in the AC map than in the HL one. Both p.d.f.'s are centered more or less near the zero values which means that the maps do not demonstrate pronounced large-scale features. The p.d.f.'s for the Galactic plane GP are substantially non-Gaussian, much wider then the previous ones, due to strong, extended emission in this region.

The polarized intensity PI is a positively defined quantity. The modulus of a Gaussian random vector follows the Rice distribution (Wardle & Kronberg 1974). So, the better Q and U correspond to a Gaussian p.d.f., the better the resulting PI distribution can be fitted by a Rice distribution (in our examples, it is the HL region). The typical width of the p.d.f. for PI grows with the widths of p.d.f.'s for the Stokes parameters.

We conclude that the shape of the p.d.f. reflects the structure of the map. A more specific quantification of the p.d.f. requires some appropriate quantities. The mean value $\overline{Q} = \int Qp(Q)\mathrm{d}Q$ gives a point where the p.d.f. for Q is centered. The width of the corresponding distribution is given by the standard deviation $\Delta Q = (\int (Q - \overline{Q})p(Q)\mathrm{d}Q)^{1/2}$. More precise the shape of the p.d.f. is given by the so-called skewness a and kurtosis (flatness) γ. These quantities can be presented in terms of the n-th central statistical momenta of Q, i.e. $M_n(Q) = \int (Q - \overline{Q})^n p(Q)\mathrm{d}Q$. Then

$$a = \frac{M_3}{M_2^{3/2}}, \qquad \gamma = \frac{M_4}{M_2^2} - 3\,. \tag{1}$$

The skewness a gives the asymmetry of the distribution and is equal to zero for any even p.d.f. The kurtosis γ characterizes the role of the tails in the distribution: the higher is the contribution of the tails, the larger is the value of γ. For a Gaussian distribution $a = \gamma = 0$, for the square of a Gaussian random quantity with zero mean $a = 2.8, \gamma = 12$. In the case of the high latitude region the Q and U maps give a p.d.f. which is very close to a Gaussian distribution while the p.d.f. for the Galactic plane diverges from Gaussian (compare a and γ in Table 2). The table demonstrates that statistical properties obtained from p.d.f. vary considerably.

Note that the p.d.f. does not give any information concerning the scales of structures in the map. The same p.d.f. (Gaussian, for instance) can correspond to a white (delta-correlated in space) noise, or to a well structured map. To separate the contributions from small-scale noise, from

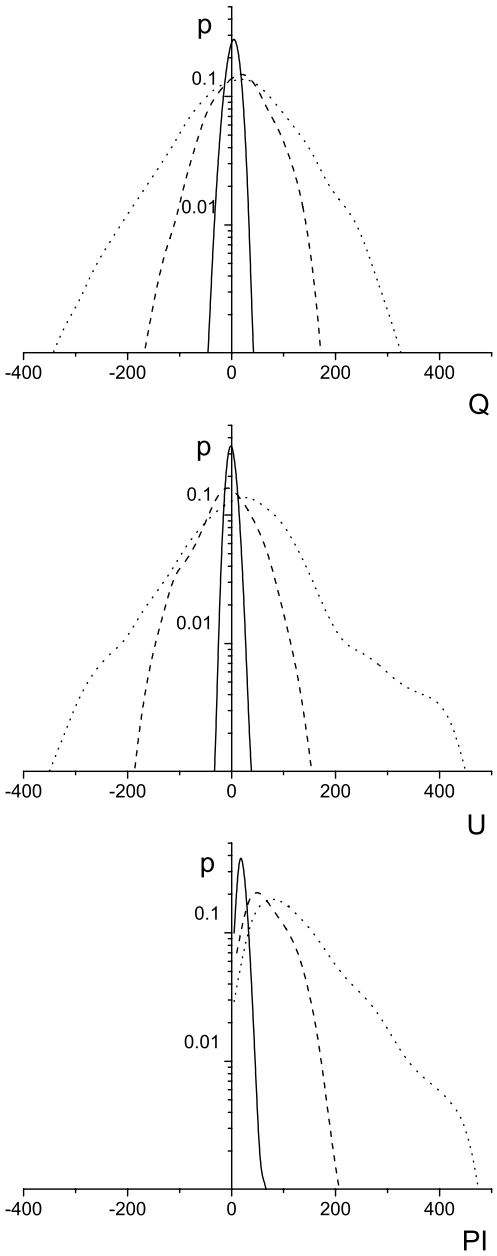

Fig. 4 P.d.f. of original Q (upper panel), U (middle panel) and PI (lower panel) maps for three regions. Solid lines correspond to the high latitude region HL, dashed lines are for the anticenter region AC and dots stand for Galactic plane GP. The intensities on the x-axes are in mK.

large-scale fields associated with absolute calibration and from discrete sources one has to consider the spectral properties of the observed maps.

3.2 Spectra

The spectral analysis is a commonly used tool for studies of scaling properties of chaotic (e.g., turbulent) fields. The spectral energy density $E(k)$ includes the energy $F(\boldsymbol{k}) = |\hat{Q}(\boldsymbol{k})|^2$ of all Fourier harmonics with wavenumbers $\boldsymbol{k}$, for which $|\boldsymbol{k}| = k$,

$$E(k) = \int_{|\boldsymbol{k}|=k} F(\boldsymbol{k}) \mathrm{d}\boldsymbol{k} \, . \tag{2}$$

Here the 2D Fourier transform $\hat{Q}(\boldsymbol{k})$ of the function $Q(\boldsymbol{x})$ is defined as

$$\hat{Q}(\boldsymbol{k}) = \int_{-\infty}^{+\infty} \int_{-\infty}^{+\infty} Q(\boldsymbol{x}) e^{-i\boldsymbol{k}\boldsymbol{x}} \mathrm{d}\boldsymbol{x} \tag{3}$$

and $\boldsymbol{x}$ is a point on the sky plane. Again, we define the spectrum in terms of Q while the definition is obviously applicable to U and PI.

Strictly speaking, the Fourier transform is developed for periodic boxes or fields in an infinite space while we are dealing with maps in a finite region. An appropriate technique for a finite region with arbitrary boundary conditions is given by wavelet analysis (see the discussion in astronomical context presented by Frick et al. 2001).

Wavelets are a tool for data analysis based on self-similar functions which are well localized both in the physical and Fourier spaces. Wavelet transformation can be considered as a generalization of the Fourier transformation, which also uses oscillatory functions, but in contrast to the Fourier transform these functions rapidly decay towards infinity. The family of functions is generated by dilations and translations of the "mother" function, called the analyzing wavelet. This procedure provides self-similarity, which distinguishes the wavelet technique from the windowed Fourier transformation, where the frequency, the width of the window and its position are three independent parameters. An extended description of the continuum wavelet transform can be found in e.g. Holschneider (1995) or Torresani (1995).

In the two-dimensional case the continuous wavelet transform can be written in the form

$$W(a, \boldsymbol{x}) = \frac{1}{a^{3/2}} \int_{-\infty}^{+\infty} \int_{-\infty}^{+\infty} Q(\boldsymbol{x}') \psi^* \left(\frac{\boldsymbol{x}' - \boldsymbol{x}}{a} \right) \mathrm{d}\boldsymbol{x}'. \tag{4}$$

Here $\boldsymbol{x} = (x, y)$, $\psi(\boldsymbol{x})$ is the analyzing wavelet (real or complex, * indicates the complex conjugation), a is the scale parameter.

In the wavelet representation the scale distribution of energy can be characterized by the *wavelet spectrum*, defined as the energy of the wavelet coefficients of scale a of the whole physical plane

$$M(a) = \int_{-\infty}^{+\infty} \int_{-\infty}^{+\infty} |W(a, \boldsymbol{x})|^2 \mathrm{d}\boldsymbol{x} \, . \tag{5}$$

The wavelet spectrum can be related to the Fourier spectrum. In the isotropic case

$$M(a) = \frac{a}{8\pi^3} \int_0^{\infty} E(k) |\hat{\psi}(ak)|^2 \mathrm{d}k \, . \tag{6}$$

This relation shows that the wavelet spectrum is a smoothed version of the Fourier spectrum, and depends on

the spectral resolution of the analyzing wavelet ψ (e.g. Frick et al. 2001). This means that the choice of the analyzing wavelet is a very important point. Any wavelet is characterized by its spatial and spectral resolution. The Fourier transform can be considered as one limiting case of wavelet transform, which uses as analyzing wavelet the harmonic. Then the analyzing wavelet has the best spectral resolution but the worst spatial one (the harmonic stretches from $-\infty$ to $+\infty$). In the other limit a difference of two delta-functions ($\psi(x) = \delta(x) - \delta(x-1)$) can be used as the analyzing wavelet (which corresponds to the calculation of a second order structure function). Then one gets the best spatial resolution but the worst spectral resolution (it means that the structure function gives a very smooth dependence of the scale which can look like a power law function even if the spectrum is very irregular and no smooth spectral energy distribution exists at all). All other wavelets are in between of these two cases. Wavelet spectra shown below, are obtained using the PH wavelet (Frick et al. 2001), which is localized in Fourier space in a ring with a median radius 2π and vanishes for $|\boldsymbol{k}| < \pi$ and $|\boldsymbol{k}| > 4\pi$. This wavelet provides a good compromise for spatial and spectral resolution. A detailed discussion of advantages and disadvantages of different methods of spectral analysis was already given (Frick et al. 2001).

The smallest scale (the highest frequency) of a Fourier spectra requires two pixels per period for, while the smallest scale of a wavelet spectrum, $a_{\rm w}$, is determined by the minimal number of pixels on which the analyzing wavelet can be defined with zero mean value. Thus, a wavelet spectrum starts at larger scale than the corresponding Fourier spectrum. In practice, the size of the beamwidth, $a_{\rm b}$, determines the smallest relevant scale (or $a_{\rm w}$ if $a_{\rm w} > a_{\rm b}$). From the large-scale side the range of relevant scales is limited by about half of the smallest side of the map.

The wavelet spectra of the original Q, U and PI maps are shown in Fig. 5 for the regions AC, GP and HL. In the small-scale part of the spectra quite pronounced power-law ranges occur that are typical for turbulent media. The physical interpretation of such spectra is rather complicated because the Stokes parameters Q and U, and especially PI, are related to physical parameters of the magnetized interstellar medium in a nontrivial way (see Sect. 5). First it is important to prove that the slopes are associated with real properties of Stokes parameter distributions rather than with data processing steps applied (see Sect. 4). An other point to be clarified is the origin of peculiar features of the spectra presented. For instance, the spectrum of polarized intensity for the AC map (Fig. 5) shows a pronounced increase at large a, while the PI spectrum for the HL map has two maxima, or a minimum at $a \sim 100$. We have to find out, whether these features have a physical background or emerge as artifacts from the data processing.

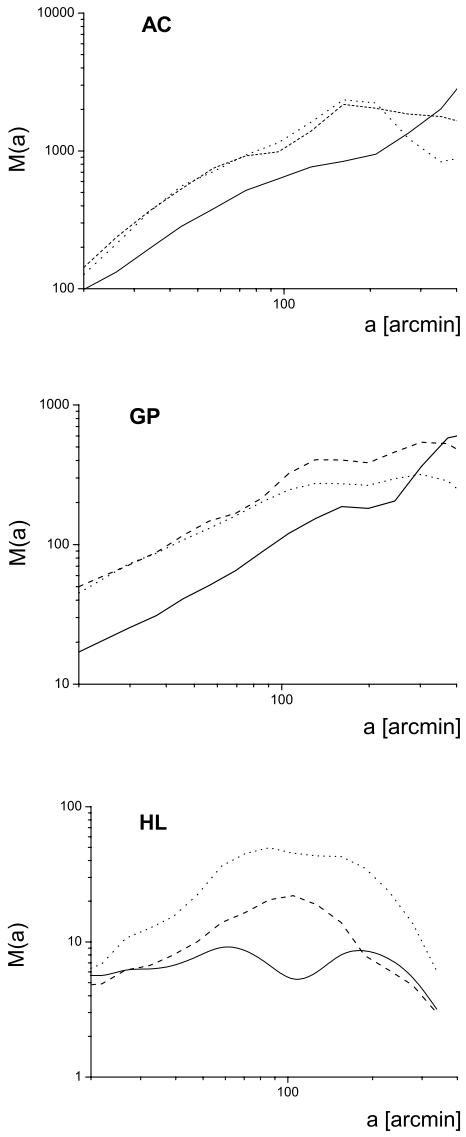

Fig. 5 Wavelet spectra of the original data for AC (upper panel), GP (middle panel) and HL (lower panel) : Q – dotted lines, U – dashed lines, PI – solid lines. $M(a)$ is the spectral energy.

4 Data treatment procedures

Three procedures will be discussed: absolute calibration, source subtraction and "denoising". Below we will mark the absolutely calibrated maps by the subscript "c", maps with sources subtracted – by the subscript "s" and "denoised" maps by "d".

4.1 Absolute calibration

Synthesis telescopes and single-dish telescopes are limited in measuring polarized structures exceeding the size of the image. Unlike for total intensities where missing large-scale emission basically introduces an offset in intensity, missing

Table 2 Characteristics of the p.d.f. for the different regions and processing steps. Indices mean: c = absolutely calibrated, s = polarized sources subtracted, d = denoised maps (see Sect. 4).

	MAP	Mean	Standard deviation	Skewness a	Kurtosis γ
AC	Q	14	54	-0.13	0.33
	U	-9.4	54	-0.20	0.32
	PI	69	38	0.73	0.74
	$PI_{\rm d}$	68	39	0.66	0.67
AC_c	$Q_{\rm c}$	-21	51	-0.06	0.58
	$U_{\rm c}$	55	64	0.087	-0.18
	$PI_{\rm c}$	90	46	0.69	0.68
	$PI_{\rm cd}$	90	47	0.64	0.64
GP	Q	11	98	-0.17	0.81
	U	20	110	0.24	1.8
	PI	120	82	1.3	2.0
	$PI_{\rm d}$	120	82	1.3	1.93
GP_c	$Q_{\rm c}$	310	98	-0.37	0.85
	$U_{\rm c}$	99	110	-0.14	1.3
	$PI_{\rm c}$	350	91	0.18	0.55
	$PI_{\rm cd}$	350	91	0.18	0.55
HL	Q	2.8	14	0.8	11.2
	U	-0.6	10.5	2.9	43
	PI	14.3	9.8	7.6	151
	$PI_{\rm d}$	8.3	13	3.6	53
	$Q_{\rm s}$	2.5	11	-0.20	0.76
	$U_{\rm s}$	-0.6	8.4	0.24	0.49
	$PI_{\rm sd}$	7.8	11.3	0.28	-0.21
HL_c	$Q_{\rm c}$	24	19	0.24	2.4
	$U_{\rm c}$	78	12	2.4	28
	$PI_{\rm c}$	83	9.1	1.2	17.3
	$PI_{\rm cd}$	83	9.2	1.2	16.9
	$U_{\rm cs}$	78	11	-0.42	0.24
	$Q_{\rm cs}$	23	18.1	-0.13	-0.45
	$PI_{\rm cs}$	83	8.4	-0.21	3.4

polarized components change the level *and* the morphology of polarized intensities, as well as the polarization angles. Therefore, missing spacing in Q and U must be added for a proper interpretation. The 1.4 GHz Effelsberg maps were complemented by large-scale emission structures from smaller telescopes (Uyaníker et al. 1998). The details for our sample maps were given in Sect. 2.

To analyze the contribution of absolute calibration we present the sequence of maps in Figs. 1–3. Maps of Stokes parameters Q and U observed by the Effelsberg antenna are shown in the left columns, (first and second row), and the corresponding PI maps are shown in the third row of the corresponding column. The calibrated $Q_{\rm c}$ and $U_{\rm c}$ maps and the corresponding $PI_{\rm c}$ map are shown in the middle column (rows 1–3). The maps of absolute calibration applied to Q and U are shown in the right column (rows 1–2). The map in the third row of the right column shows the difference of PI maps, presented in the first and in the second columns. Although the Q and U maps of absolute calibration possess only large scales, the corrections affect all scales in $PI_{\rm c}$. Hence, the nonlinear relation between Q, U and PI requires very accurate interpretation of individual details visible on absolutely calibrated maps of polarized intensity.

The effect of absolute calibration on the p.d.f. for the GP region is shown in Fig. 6. The calibration shifts the p.d.f. of Stokes parameters (the parameter U is shown as an example) but the shape remains almost stable. The shape of the p.d.f. for $PI_{\rm c}$, however, is substantially modified. The initial p.d.f. is almost a Rice distribution while after calibration the p.d.f. becomes much closer to a Gaussian (the skewness and the kurtosis are reduced from $a = 1.3$, $\gamma = 2.0$ to $a = 0.18$ and $\gamma = 0.55$). Table 2 shows the extreme values of a and γ for the region HL – the initial map of U is characterized by the skewness $a = 2.9$ and the kurtosis $\gamma = 43$, and the map of PI has $a = 7.6$ and $\gamma = 151$. Note, that in this case the absolute calibration itself also reduces the values of skewness and kurtosis, but they remain far from Gaussian ($PI_{\rm c}$ has $a = 1.2$, $\gamma = 17$). The reason is that in this case the high value of the kurtosis is determined mainly by discrete sources (see Sect. 4.2).

The effect of absolute calibration on the spectra is shown in Fig. 7 for the high-latitude region HL. The spectra of Stokes parameters $U_{\rm c}$ and $Q_{\rm c}$ are affected at large scales only. The original spectral turn-over vanishes by the calibration process. The large-scale part of the U and Q spectra moved up and the spectral slope continues for scales $a > a_{\rm c} \approx 90'$. These contributions to the large scales of $Q_{\rm c}$ and $U_{\rm c}$ spectra result in corresponding additional energy in the $PI_{\rm c}$ spectrum, but this energy is distributed over a larger range of scales. The spectrum of calibrated $PI_{\rm c}$ obtains a maximum at scale $a \approx 120'$, while the spectra of calibrated Stokes parameters have maxima at scales of about $240'$ (cf.: the scale of $|\sin x|$ is two times lower than that of $\sin x$).

The results for the two other sky regions confirm that the absolute calibration does not substantially affect the small-scale part of the spectra (Fig. 8). The calibrated maps show homogeneous gradients and basically unchanged $Q_{\rm c}$ and $U_{\rm c}$ spectra. The absolute calibration generally raises the amplitudes of the $PI_{\rm c}$ spectra. For the GP region the small-scale (power-law) part of the spectrum increases uniformly (the slope does not change), but the absolute calibration leads to a significant decrease in the power at the largest scales. In AC a bump arises at scales of about 150–200′.

4.2 Source subtraction

Observations include all emission components along the line of sight and thus also objects not related to the interstellar medium under investigation. In our case strong polarized extragalactic radio sources can significantly change the spectral properties of Galactic polarized emission. They can be subtracted using a Gaussian fitting procedure.

Isolated polarized sources occupy a small part of a map and their subtraction practically does not change the central part of the p.d.f. shown in Fig. 4, but their contribution to high-order momenta (see Sect. 3.1) can be dominant. For

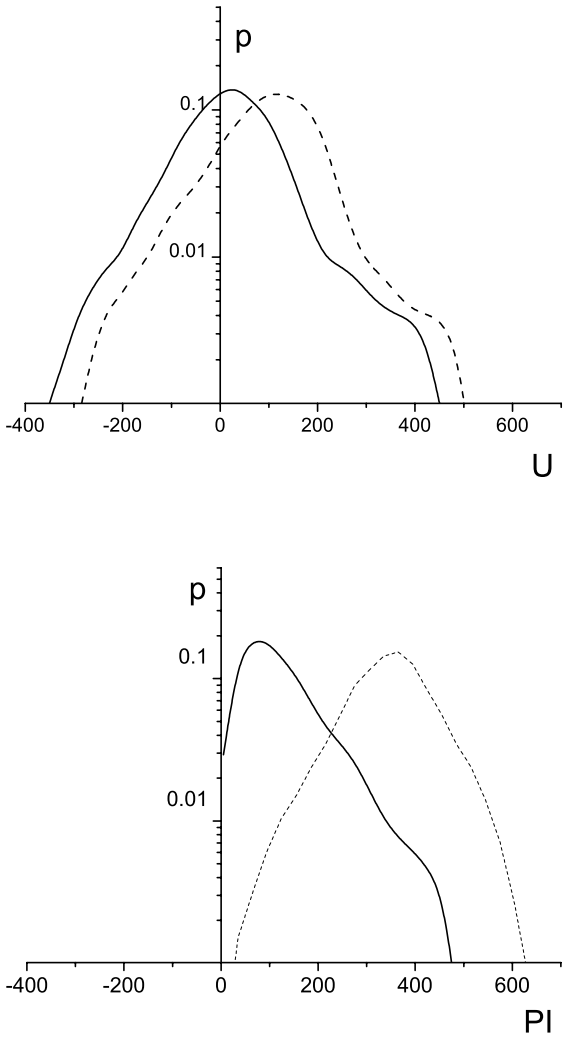

Fig. 6 P.d.f. of U (upper panel) and PI (lower panel) of observed (solid line) and absolutely calibrated (dashed line) data for the map GP.

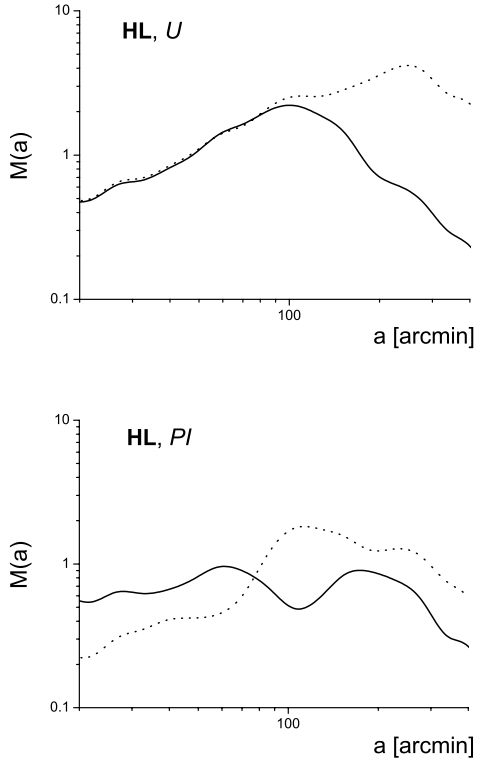

Fig. 7 The effect of absolute calibration: Wavelet spectra for the region HL: upper panel – U, lower panel – PI. Original spectra – solid lines, calibrated – dotted lines.

example, by subtracting three sources from the HL map, one reduces the value of the kurtosis from $\gamma = 53$ to $\gamma = -0.2$ (Table 2).

Source subtraction can strongly affect the spectral properties of a map of diffuse emission, where they act like delta functions and contribute to a large part of the spectral range. Thus, source subtraction leads to a reduction of the small-scale amplitudes of the spectrum. The effect is most pronounced in the HL spectra of U (see the upper panel in Fig. 9). For the HL Q and U spectra a pronounced change of their slopes is seen: the initial slopes of 1.4 and 0.9 change to 1.9 and 1.4 after source subtraction. The spectral slope of $PI_{\rm s}$ changes from 0.5 to 0.9. Note that there are only 3 sources in the HL map, which is $5^\circ \times 5^\circ$ in size. For larger maps with a larger number of sources the influence of sources can be even stronger. Also unresolved polarized sources may contribute in this way. Quantitative estimates are not possible yet, since the confusion level for polarized sources is not known.

At low latitudes (AC and GP maps), however, discrete sources practically do not influence the spectral properties. The reason is that in the Galactic plane the diffuse polarized emission is rather strong in comparison to that from the sources. Thus for the weak diffuse emission of the HL region out of the plane the influence of strong sources on the spectral properties is significant.

4.3 "Denoising"

The Gaussian distribution in the observed Stokes parameters Q and U results in a Rice distribution in PI. Because the latter one is asymmetric, a Gaussian uncertainty in the observed quantities leads to a positive bias in PI. The aim of "denoising"[1] is to restore the Gaussian nature of noise in PI. But the denoising also changes the structures in the map.

In practice, the denoising is a positive bias correction (Wardle & Kronberg 1974). One tries to restore the Gaussian probability distribution function of PI, introducing a "denoising" term, ξ, in the right-hand part of the relation

$$PI_{\rm d}^2 = (Q_{\rm s} + C_Q)^2 + (U_{\rm s} + C_U)^2 - \xi^2, \qquad (7)$$

[1] The expression "denoising" is widely used but misleading, because the noise is not reduced (see Sect. 5).

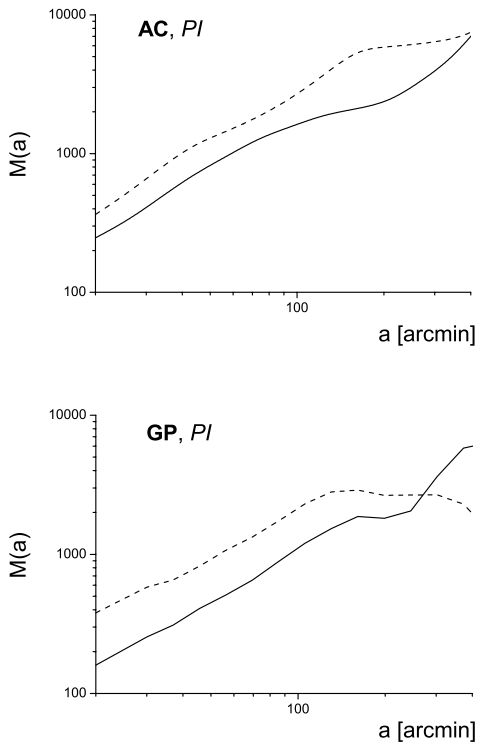

Fig. 8 The effect of absolute calibration: Wavelet spectra for the region AC (upper panel) and for the region GP (lower panel). PI – solid lines, $PI_{\rm c}$ – dashed lines.

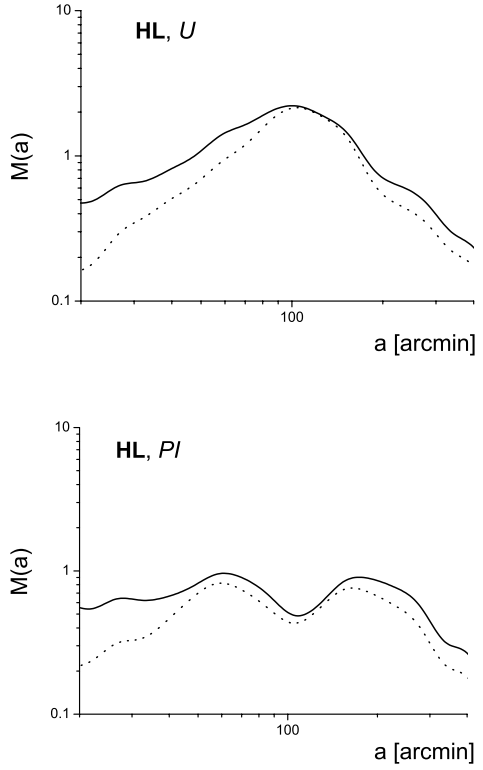

Fig. 9 The effect of source subtraction: Wavelet spectra for the region HL: U – upper panel, PI – lower panel.

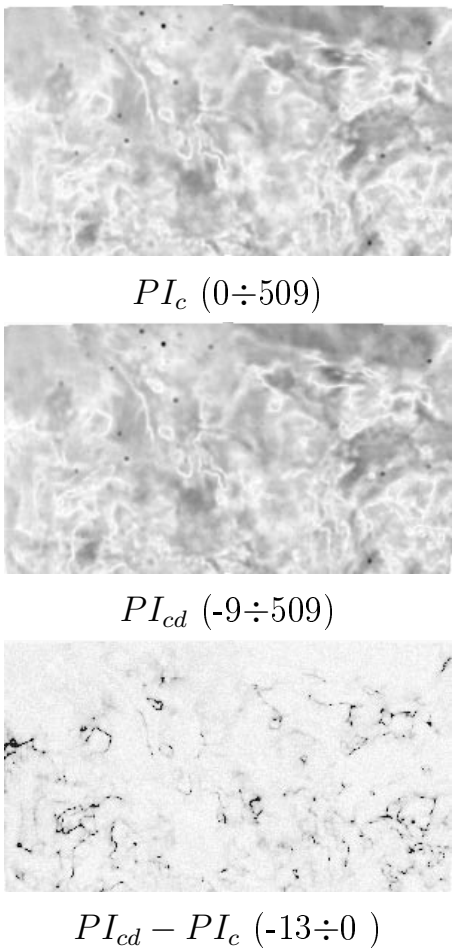

Fig. 10 The calibrated PI map for the region AC before (upper panel) and after (middle panel) denoising. The difference is shown in the lower panel.

where $PI_{\rm d}$ is the corrected polarized intensity, $Q_{\rm s}$ and $U_{\rm s}$ are the maps with sources subtracted, C_Q and C_U are the absolute calibration components. $\xi \simeq 1.2\sigma$ where σ is the mean rms noise in the Q and U maps. If the correction term is larger than $(Q_{\rm s}+C_Q)^2+(U_{\rm s}+C_U)^2$, $PI_{\rm d}^2$ becomes negative. In this case the $PI_{\rm d}$ is formally defined as negative

$$PI_{\rm d} = -\sqrt{|(Q_{\rm s}+C_Q)^2+(U_{\rm s}+C_U)^2-\xi^2|}\,. \qquad (8)$$

The result of denoising is shown in Fig. 10, where the calibrated AC map, the denoised one and their difference are presented. The latter map shows only rather weak structures (the amplitude does not exceed 3% of the amplitude of the $PI_{\rm c}$ map). Discrete (black) pixels indicate negative (nonphysical) values in the $PI_{\rm d}$ map resulting from Eq. (8).

The change of the p.d.f. is illustrated in Fig. 11 by the example of region HL. The probability distribution of slightly shifts to smaller values of PI getting a prolongation in the domain of negative PI with a sharp cutoff at $PI_{\rm d} = -\xi$.

Figure 12 illustrates the influence of the denoising procedure on the original PI spectrum of the HL region. In the HL region the noise level is just a few times weaker than the

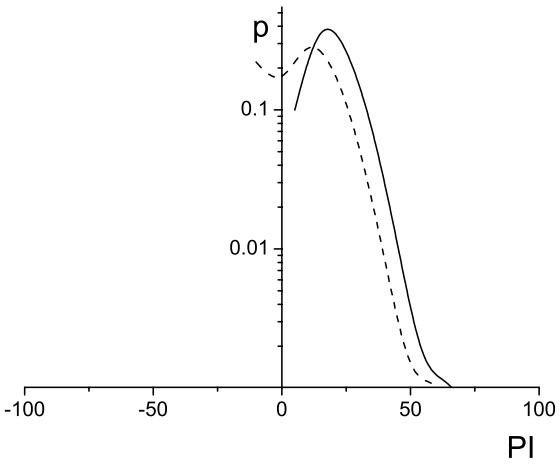

Fig. 11 The effect of denoising: p.d.f. of original (solid line) and denoised (dashed line) PI for the region HL.

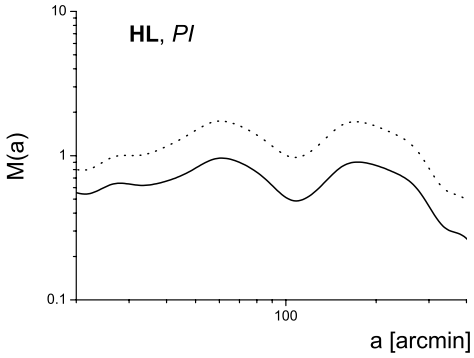

Fig. 12 The effect of denoising: Wavelet spectra for the region HL: original map – solid line, denoised map – dashed line.

emission structures. Denoising shifts up the whole spectrum of the original data; thus by denoising one adds energy to all scales. For the previously calibrated PI map, however, the $PI_{\rm c}$ level is much larger than the noise level and the denoising process does not significantly change the spectrum.

5 Discussion

We attempted to separately discuss the effects of various procedures such as absolute calibration, source subtraction and denoising applied to radio polarization maps. We conclude that absolute calibration affects mainly the large-scale emission, whereas source subtraction may change the small-scale part of the spectrum. Denoising does not vary the spectral energy distribution, but may change the entire energy level. As an example of a resulting spectrum of Stokes parameters we present in Fig. 13 the final spectrum of the U map of the HL region after absolute calibration and source subtraction. The original spectrum is also

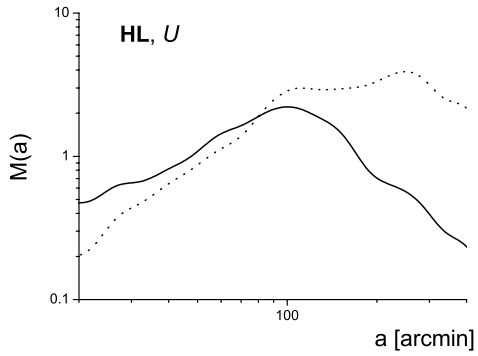

Fig. 13 Original (solid) and final (dashed) wavelet spectrum for the map U of the region HL.

shown for comparison. The latter differs from the former over the entire range of scales. Comparing this plot with Figs. 7 and 9, the effects of absolute calibration and source subtraction are clearly separated by the scale $a \approx 80'$. The role of subtracted isolated sources monotonically increases with decreasing scales leading to a change of the spectral slope, while the absolute calibration introduces energy on the large-scale part of the spectrum.

We note that the subtraction of just a few intense polarized sources can substantially affect the spectral slope at small scales which are of interest for the study of turbulent interstellar media. Hence, proper source subtraction is a crucial issue of data processing for maps of diffuse polarized emission. This problem will be even more severe for observations with higher sensitivity and angular resolution, where compact sources become more pronounced compared to diffuse structures. The problem of spectral distortions by compact sources was stressed in the context of an investigation of the influence of Galactic foreground emission on studies of the cosmic microwave background (CMB) by La Porta & Burigana (2006).

Following Simmons & Stewart (1985) we note that in principle two options of data presentation are possible. The data may be presented in the traditional form of PI maps and one might study the p.d.f. and/or spectral characteristics. An obvious disadvantage is the positive bias in PI and the non-Gaussian nature of the noise in PI maps. Alternatively, the data may be presented in terms of Stokes parameters Q and U (or in terms of complex polarized intensity $\mathcal{P} = Q + iU$, Burn 1966). The advantage is the Gaussian nature of noise for Q and U. The problem is that the particular Q and U distributions depend on the choice of the instrumental and astronomical coordinate systems, which in principle are arbitrary. On the contrary, PI characterizes the ISM properties and does not depend on the coordinate systems. For a given absolute calibration one can easily predict the change in the spectral properties of Q and U maps due to the linearity of the Fourier transform. However, absolute calibration causes more complicated spectral modifications in PI.

A possible compromise between the two approaches described above is given by the "denoising" procedure. Denoising adds some moderate additional noise in the PI maps to obtain an almost Gaussian noise distribution and $< PI >= 0$ in a region without signal. The price to be paid for that is the non-physical negative values of PI which arise in regions of low or no polarization. These non-physical regions produce an extension of the p.d.f. at negative PI (see Fig. 11). The denoising process does not lead to any dramatic changes in the PI spectrum, although some additional energy from the artificial (almost white) noise is added. In this respect, the conventional wording "denoising" is not appropriate – the procedure does not reduce the noise at all. The term "debiasing" corresponds much better to the procedure, because the intention is to just compensate the positive bias in PI.

It is rather unexpected that moderate denoising can provide a significant growth of the spectral energy. The maximum correction in the case of AC, shown in Fig. 10, does not exceed 3% of the maximum value in the calibrated PI map. In the case of the region HL the correction is slightly higher (up to 5% of the maximum values of the original map), but Fig. 12 shows that the total energy increases by a factor of about 40%. This is because the maximum values in this map correspond to rare isolated points only and the average diffuse emission is weak. We also stress that the spectral energy of a PI map, being formally similar to the spectral energy of a turbulent velocity field, is not associated with any conserved quantity like total energy. Therefore, naive expectations based on the energy conservation argument are misleading here.

The effects of data processing on statistical properties of the maps are clear enough to consider the spectra and p.d.f.'s obtained from the resulting maps as a valuable source of information concerning the physical properties of the magnetized interstellar medium. The spectra obtained contain power-law like ranges at small scales (Figs. 13 and 14). The slopes of the spectra are a usual topic for discussion in the theory of turbulence. The final spectrum of U for the HL region shown in Fig. 13 reveals at scales $a < 100$ arcsec a slope close to the famous 5/3, common for the conventional Kolmogorov theory of turbulence. We stress that a direct identification of the slope as a Kolmogorov one is misleading because the Q and U spectra do not reproduce turbulent spectra in a straightforward way. The way to a physical interpretation of the spectral indices of Stokes parameters or PI is to simulate the corresponding distribution for an artificial random magnetic field produced by a random value generator in a 3D cube (Fletcher et al., in prep.). A better approach would be to use the results of direct numerical simulations (DNS) of the Galactic magnetized interstellar medium (Korpi et al. 1999; Gazol et al. 2001).

The spectra for the Galactic plane region GP are much flatter than the corresponding ones for the HL region. We show the spectra of Q, U and PI for the GP region in the middle panel of Fig. 14 and conclude that for $a < 100'$

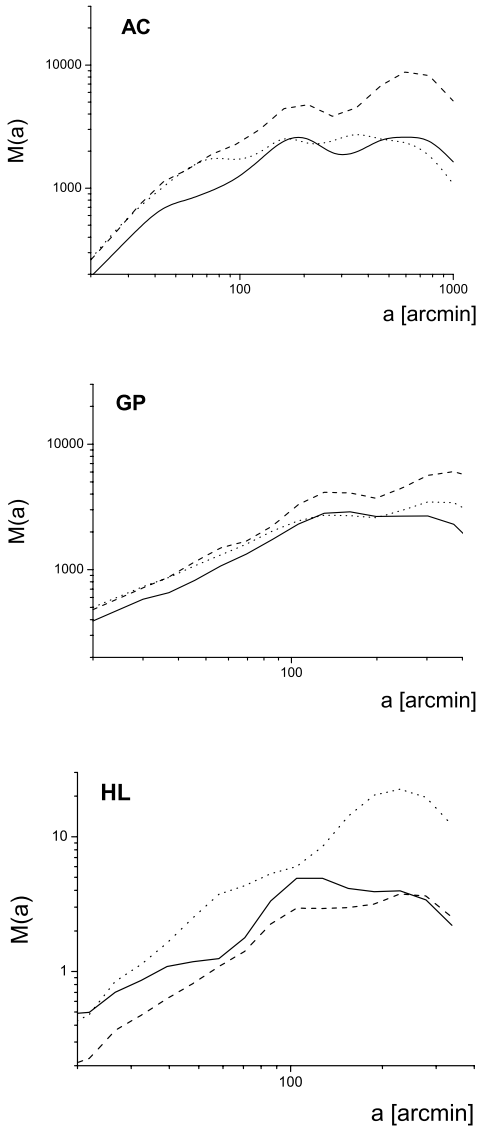

Fig. 14 Final wavelet spectra for AC (upper panel), GP (middle panel) and HL (lower panel) : Q – dotted lines, U – dashed lines, PI – solid lines.

the slopes are about 0.9–1.2 which seems too low for turbulent spectra. We believe that the slopes are associated with remote structures of large-scale magnetic fields or thermal electron density. For the region AC (upper panel of Fig. 14) the small-scale range of the spectra is divided in two parts: for $a < 50'$ the slopes are close to 5/3 while for $50' < a < 200'$ they are about 1.

Finally, let us note that small-scale ISM turbulence should provide random homogeneous isotropic distributions of Q and U. Hence, the correlation between Q and U taken at the same location is expected to vanish. Detection of noticeable cross-correlation at a given scale indicates that some isolated features make an essential contribution to the observed emission. At large scales a relationship of Stokes parameters is expected because the regular large-scale mag-

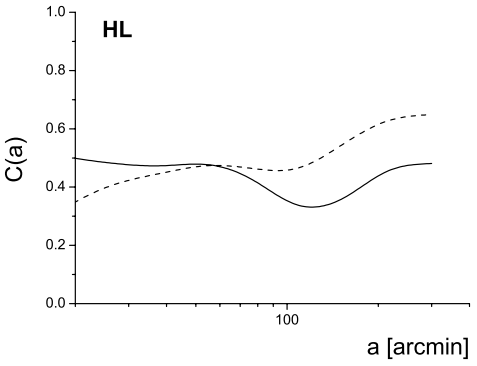

Fig. 15 Wavelet cross-correlation for Q and U for the region HL: original data (solid) and calibrated data after source subtraction (dashed).

netic field and variations in thermal electron density can produce correlated variations of both variables.

We verify the above concept using the correlation coefficient for a given scale a that can be defined as

$$C(a) = \frac{\int\int W_Q(a,\boldsymbol{x}) W_U^*(a,\boldsymbol{x}) \mathrm{d}\boldsymbol{x}}{[M_Q(a) M_U(a)]^{1/2}} \,. \quad (9)$$

In Fig. 15 the wavelet cross-correlation function $C(a)$ is shown for the original maps Q and U (for the region HL) and for the maps obtained after absolute calibration and source subtraction. The visible changes are consistent with the above conclusions. The wavelet cross-correlation function is almost flat for the original maps. The source subtraction essentially reduces the level of correlation at small scales (left-hand part of the curve) because the bright sources provide the correlations at small scales. The influence of these sources monotonically decreases with increasing scale. At large scales the effect of absolute calibration becomes noticeable and increases the level of correlation (right-hand part of the curve in Fig. 15).

Acknowledgements. This work was supported through the grant DFG 436 RUS 113/772 – RFBR 03-02-04031. The authors wish to thank Elly Berkhuijsen, Anvar Shukurov and Rodion Stepanov for useful discussions and many helpful comments. Based on observations with the 100-m telescope of the MPIFR (Max-Planck-Institut für Radioastronomie) at Effelsberg.

References

Beck, R.: 2006, in: F. Boulanger, M.A. Miville-Deschenes (eds.), *Polarization 2005*, in press (astro-ph/0603531)
Beck, R., Brandenburg, A., Moss, D., Shukurov, A., Sokoloff, D.: 1996, ARAA 34, 155
Brouw, W. N., Spoelstra, T. A. Th.: 1976, A&AS 26, 129
Burn, B. J.: 1966, MNRAS 133, 67
Duncan, A. R., Haynes, R. F., Jones, K. L., & Stewart, R. T.: 1997, MNRAS 291, 279
Fletcher, A., Shukurov, A.: 2006, in: F. Boulanger, M.A. Miville-Deschenes (eds.), *Polarization 2005*, in press (astro-ph/0602536)
Frick, P., Beck, R., Berkhuijsen, E. M., Patrickeyev, I.: 2001, MNRAS 327, 1145
Gaensler, B. M., Dickey, J. M., McClure-Griffiths, N. M., Green, A. J., Wieringa, M. H., Haynes, R. F.: 2001, ApJ 549, 959
Gazol, A., Vázquez-Semadeni, E., Sánchez-Salcedo, F. J., Scalo, J.: 2001, ApJ 557, L121
Gray, A. D., Landecker, T. L., Dewdney, P. E., Taylor, A. R.: 1998, Nature 393, 660
Haverkorn, M., Heitsch, F.: 2004, A&A 421, 1011
Haverkorn, M., Katgert, P., de Bruyn, A. G.: 2003a, A&A 403, 1031
Haverkorn, M., Katgert, P., de Bruyn, A. G.: 2003b, A&A 403, 1045
Haverkorn, M., Katgert, P., de Bruyn, A. G.: 2004, A&A 427, 549
Holschneider, M.: 1995, *Wavelets: An Analysis Tool*, Oxford University Press, Oxford
Korpi, M. J., Brandenburg, A., Shukurov, A., Tuominen, I., Nordlund, Å.: 1999, ApJ 514, L99
La Porta, L., Burigana, C.: 2006, A&A, in press (astro-ph/0601371)
Reich, W.: 1982, A&AS 48, 219
Reich, W.: 2006, in: R. Fabbri (ed.), *Cosmic Polarization*, Research Signpost, in press (astro-ph/0603465)
Reich, P., Reich, W.: 1986, A&AS 63, 205
Reich, P., Reich, W., Fürst, E.: 1997, A&AS 126, 413
Reich, W., Fürst, E., Reich, P., Wielebinski, R., Wolleben, M.: 2002, in: S. Cecchini, S. Cortiglioni, R. Sault, C. Sbarra (eds.), *Astrophysical Polarized Backgrounds*, AIP Conf. Proc. 609, p. 3
Reich, W., Fürst, E., Reich, P., Uyaníker, B., Wielebinski, R., Wolleben, M.: 2004, in: B. Uyaníker, W. Reich, R. Wielebinski (eds.), *The Magnetized Interstellar Medium*, p. 45
Scheuer, P. A. G., Hannay, J. H., Hargrave, P. J.: 1977, MNRAS 180, 163
Shukurov, A., Berkhuijsen, E. M.: 2003, MNRAS 345, 1392
Simmons, J. F. L., Stewart, B. G.: 1985, A&A 142, 100
Sokoloff, D. D., Bykov, A. A., Shukurov, A., Berkhuijsen, E. M., Beck, R., Poezd, A. D.: 1998, MNRAS 299, 189
Torresani, B.: 1995, *Continuous Wavelet Transform*, Savoire, Paris
Uyaníker, B., Fürst, E., Reich, W., Reich, P., Wielebinski, R.: 1998, A&AS 132, 401
Uyaníker, B., Fürst, E., Reich, W., Reich, P., Wielebinski, R.: 1999, A&AS 138, 31
Wardle, J. F. C., Kronberg, P. P.: 1974, ApJ 194, 249
Wolleben, M.: 2005, PhD thesis, University of Bonn
Wolleben, M., Landecker, T. L., Reich, W., Wielebinski, R.: 2006, A&A 448, 411